Two-photon-induced x-ray emission in neon atoms

Yu-Ping Sun,[1,2,*] Zilvinas Rinkevicius,[2] Chuan-Kui Wang,[1,2] Stephane Carniato,[3,4]
Marc Simon,[3,4] Richard Taïeb,[3,4] and Faris Gel'mukhanov[2]

[1]*College of Physics and Electronics, Shandong Normal University, 250014 Jinan, China*
[2]*Theoretical Chemistry, School of Biotechnology, Royal Institute of Technology, S-10691 Stockholm, Sweden*
[3]*Laboratoire de Chimie Physique Matière et Rayonnement, Université Pierre et Marie Curie Université Paris 06, Unité de Mixte de Recherche (UMR) 7614, F-75005 Paris, France*
[4]*Laboratoire de Chimie Physique Matière et Rayonnement, Centre National de la Recherche Scientifique, UMR 7614, F-75005 Paris, France*

(Received 26 July 2010; published 25 October 2010)

We investigated the resonant x-ray emission from a neon atom induced by the two-photon population of a double-core-hole excited state. Two qualitatively different schemes of this process are studied: The first one involves an off-resonant intermediate single-core-hole state; the second scheme passes through a resonant core-ionized intermediate state. The numerical simulations of the resonant x-ray emission performed for different peak intensities and pulse durations show significant population of the double-core-hole final states. Therefore, rather strong two-photon absorption-induced x-ray emission is predicted for both studied schemes. Thus, high counting rates in experimental measurements are expected.

DOI: 10.1103/PhysRevA.82.043430 PACS number(s): 32.80.Aa, 32.80.Rm, 32.30.Rj

I. INTRODUCTION

The invention of the laser triggered intensive studies of nonlinear phenomena in the infrared and optical regimes [1]. Until 2009, experimental studies of nonlinear processes in shorter wavelengths were impossible, as no high brilliance x-ray source was available. Recently, novel sources of x-ray radiation, namely, the x-ray free-electron laser (XFEL) [2–5], were built, generating high-intensity radiation pulses and opening unique opportunities to study such nonlinear phenomena. Based on these developments, several interesting ideas related to the x-ray pump-probe spectroscopy have already been suggested [6–11], as well as multiple ionizations of rare gas atoms via multiphotons in the XUV regime [12]. Furthermore, various physical phenomena relevant to spectroscopic applications of the XFEL were studied in detail: a slowdown of the XFEL pulse caused by nonlinear interaction of x rays with a macroscopic medium [13–15] as well as stimulated resonant x-ray Raman scattering and four-wave mixing [13–16]. The key element of the latter applications is the high intensity of the x-ray pulse generated by the XFEL that allows the study of x-ray radiation interaction with matter in the nonlinear regime. Hence, the high intensity of the XFEL allows to significantly populate the core excited state because the Rabi frequency becomes comparable to the lifetime broadening of the core excited state. This opens the new opportunities to study the x-ray emission of the intermediate state populated by two-photon absorption (TPA).

The free-electron laser, built all around the world, can generate extremely intense coherent and short-pulsed vuv and x-ray light. They deliver up to 10^{13} photons in pulses as short as 10 fs with an energy uncertainty of $\Delta E/E$ of 10^{-3}. The peak brilliance is up to 9 orders of magnitude higher than those achieved at the most advanced third-generation synchrotron-radiation sources. Due to the small source size, the beam can be focused down to micrometer spots, and light intensities at the focus are up to 10^{18} W/cm^2. The Linac coherent-light source (LCLS) machine is designed to deliver x rays from below 0.8 up to 8 keV at 100-fs pulse duration [17]. The LCLS operates with conventional accelerator cavities at a constant repetition rate between 30 and 120 Hz. In 2010, the SPring8 compact self-amplified spontaneous emission (SASE) source will be commissioned in Japan [18] with beam parameters similar to the LCLS and a repetition rate of 60 Hz. In 2014, the XFEL in Hamburg [19] will have a photon bunch structure with 3000 photon pulses every 100 ms, equally spaced in time by 200 ns.

In order to meet some of the challenges concerning the detector instrumentation, the Max Planck Institute has designed very large pn-charge coupled device (pn-CCD) chips [20]. The pn-CCD detector can collect photons covering a large solid angle with an energy resolution of 40 to 200 eV between 100 and 25 keV, a quantum efficiency close to 1, and at a frame readout rate up to 200 Hz.

The aim of our paper is the resonant x-ray Raman scattering (RXRS) induced by the TPA. The main attention paid here is to the resonant enhancement of the TPA, and, hence, of the RXRS induced by the TPA. The process studied here relies on the formation of the double-core-hole state in a neon atom. This state was already observed in electron-impact experiments [21] in 1978, and the first theoretical description of this state was carried out earlier by Bhalla [22]. The cross sections of the double-core-hole formation via TPA were recently calculated for atoms [23–25] and molecules [26]. The first experimental observation of the TPA in the XUV region was performed on helium [27]. This year, double-core-hole formation via TPA was observed at LCLS [28–30].

The conventional experimental technique to observe x-ray TPA is photoemission [31]. Here, we suggest and study an alternative scheme based on the TPA-induced x-ray fluorescence (TPAXF) or lasing. We develop the general theory and apply it to the TPAXF of neon vapor with the frequencies of the x-ray pump of 927.7 and 984.7 eV, which

*yuping@theochem.kth.se

correspond to two different schemes. The first one is based on the $1s^2 \rightarrow 1s^1 3p \rightarrow 1s^0 3p^2$ TPA double-core-hole excitation with an off-resonant intermediate state. For the second one, we consider the following scheme: $1s^2 \rightarrow 1s^1\psi_E^1 \rightarrow 1s^0\psi_E^1 3p^1$.

The paper is organized as follows. The two different schemes of the two-photon-induced x-ray emission are described in Secs. II A and II B, while details of our numerical simulations are outlined in Sec. II C. The discussion of the TPA-induced fluorescence and population analysis are presented in Sec. III. Our findings are summarized in Sec. IV.

II. THEORETICAL MODELS

A. The kinetic model of bound-bound-bound-bound TPA

We first present the kinetic model for TPA along the scheme shown in Fig. 1(a). The first photon absorbed corresponds to the transition from the ground (bound) state $1s^2 3p^0$ to the intermediate bound state $1s^1 3p^1$. The second photon absorbed leads to the transition between the $1s^1 3p^1$ bound state and the final $1s^0 3p^2$ bound state. This TPA resonance scheme corresponds to the bound-bound-bound-bound (BBBB) TPA transition: $|0\rangle \rightarrow |1\rangle \rightarrow |2\rangle$, where $|0\rangle = 1s^2 2s^2 2p^6$, $|1\rangle = 1s^1 2s^2 2p^6 3p^1$, and $|2\rangle = 1s^0 2s^2 2p^6 3p^2$ are the ground, the intermediate, and the final states of the neon atom, respectively.

We now introduce other important elements of our kinetic model. We will use the rotating-wave approximation (RWA) assuming that the x-ray field is

$$\frac{E(t)}{2} e^{i\omega t} + \text{c.c.} \tag{1}$$

The RWA is a good approximation in the x-ray region where the photon frequency ω is much larger than the Rabi frequencies G_{nm} defined as

$$G_{nm} = \frac{d_{nm} E(t)}{2\hbar}. \tag{2}$$

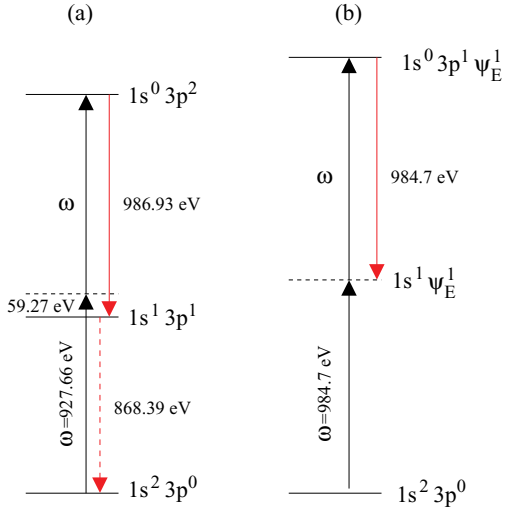

FIG. 1. (Color online) Scheme of the TPA-induced fluorescence in the Ne atom. (a) Bound-bound-bound-bound (BBBB) transitions. (b) Bound-continuum-bound-bound (BCBB) transitions. The experimental value of the 1s-ionization potential of Ne is 870.2 eV.

Here, d_{nm} is the transition dipole moment between the electronic states n and m, and $E(t)$ is the envelope of the x-ray pulse. Due to the spherical symmetry of the atom, we can arbitrarily choose the axis of quantization z. We orient the z axis along the polarization vector of the x-ray photon **e**. Due to this, only the z components of the transition dipole moments are needed.

We can then write the density-matrix equations for the BBBB-TPA transition [Fig. 1(a)] as

$$\begin{aligned}
\left(\frac{\partial}{\partial t} + \Gamma_{22}\right)\rho_{22} &= 2\,\mathrm{Im}(\rho_{21} G_{12}),\\
\left(\frac{\partial}{\partial t} + \Gamma_{11}\right)\rho_{11} &= -2\,\mathrm{Im}(G_{12}\rho_{21}) + 2\,\mathrm{Im}(\rho_{10} G_{01}),\\
\left(\frac{\partial}{\partial t} + \Gamma_{21} - i(\omega - \omega_{21})\right)\rho_{21} &= -iG_{21}(\rho_{22} - \rho_{11})\\
&\quad - i\rho_{20} G_{01},\\
\left(\frac{\partial}{\partial t} + \Gamma_{20} - i(2\omega - \omega_{20})\right)\rho_{20} &= -i(\rho_{21} G_{10} - G_{21}\rho_{10}),\\
\left(\frac{\partial}{\partial t} + \Gamma_{10} - i(\omega - \omega_{10})\right)\rho_{10} &= iG_{10}(\rho_{00} - \rho_{11}) + iG_{12}\rho_{20},\\
\frac{\partial}{\partial t}(\rho_{00} + \rho_{11} + \rho_{22}) &= -\Gamma_{22}\rho_{22} - \Gamma_{11}\rho_{11} - \gamma_{\mathrm{ph}}\rho_{00}.
\end{aligned} \tag{3}$$

The last equation describes the decrease of concentration of intact molecules due to both the Auger decays, with the rates Γ_{22}, Γ_{11}, and the direct photoionization, with the rate,

$$\gamma_{\mathrm{ph}} = \sigma_{\mathrm{ph}} S. \tag{4}$$

The modulus of the Poynting vector $S = I/\hbar\omega$ is the ratio of the light intensity $I = c\epsilon_0 |E(t)|^2/2$ by the energy of x-ray photon $\hbar\omega$. The dominant contribution in the photoionization cross section σ_{ph} comes from ionization of the K-shell electron, as the energy of the photon is close to the K-shell ionization threshold $I_{1s}(\omega - I_{1s} = 927.7 - 870.2 = 57.5$ eV, see also Sec. III). Relaxation rate of the coherence ρ_{ij},

$$\Gamma_{ij} = \tfrac{1}{2}(\Gamma_{ii} + \Gamma_{jj}) + \gamma, \qquad i \neq j \tag{5}$$

includes, in the general case, the pressure or collisional breadth [32–34] γ. These collisions (or interruptions) cause a broadening by changing the phase of the radiator, destroying the coherence with rate γ. Here, in the gas-phase system, the collisional broadening is negligible compared to Γ_{ii}. However, another kind of phase interruption can occur due to the XFEL pulse itself. In a single-path SASE XFEL where the process of amplification starts from noise, the random fluctuations of amplitude and the phase [35] of the field produce a relatively wide output radiation. These fluctuations result in a spectral broadening γ in a similar way as the collisional one [36–38], see Eq. (5). An alternative way to take the random fluctuations of the SASE XFEL field into account was developed by Rohringer and Santra in Ref. [35]. It is worth noticing that the spectral width of the XFEL pulse can be shortened using seeding radiation. For example, the two-stage XFEL [39] leads to an meV bandwidth with $\gamma/\omega \approx 10^{-6}$.

B. Kinetics of bound-continuum-bound-bound TPA

Now, we turn to the second scheme of the TPA population of the two core-hole final states [Fig. 1(b)]. The first absorbed photon corresponds to the transition between the ground bound state and the core-ionized continuum state, while the second one leads to a transition between bound states of core-ionized neon. We label this scheme the bound-continuum-bound-bound scheme (BCBB): $|0\rangle \to |1E\rangle \to |2E\rangle$, where $|0\rangle = 1s^2 2s^2 2p^6$, $|1E\rangle = 1s^1 2s^2 2p^6 \psi_E^1$, and $|2E\rangle = 1s^0 2s^2 2p^6 3p^1 \psi_E^1$ are the ground, intermediate, and final states of neon, respectively. Here, ψ_E denotes the continuum state of the electron. Note that, contrary to the BBBB scheme, the intermediate continuum state is now on-resonance with the x-ray photon.

Neglecting the weak energy dependence of the bound-continuum transition dipole moment $d_{1E0} \approx d_{10}$ (or $G_{1E0} \approx G_{10}$), we can write the density-matrix equations for this new scheme as

$$\begin{aligned}
\frac{\partial}{\partial t}(\rho_{00}+\rho_{11}+\rho_{22}) &= -\Gamma_{22}\rho_{22} - \Gamma_{11}\rho_{11},\\
\left(\frac{\partial}{\partial t}+\Gamma_{11}\right)\rho_{1E1E} &= 2\,\mathrm{Im}(\rho_{1E0}G_{01}) - 2\,\mathrm{Im}(G_{12}\rho_{2E1E}),\\
\left(\frac{\partial}{\partial t}+\Gamma_{22}\right)\rho_{2E2E} &= 2\,\mathrm{Im}(\rho_{2E1E}G_{12}),\\
\left(\frac{\partial}{\partial t}+\Gamma_{21}-i(\omega-\omega_{21})\right)\rho_{2E1E} &= iG_{21}[\rho_{1E1E}-\rho_{2E2E}]\\
&\quad - i\rho_{2E0}G_{01},\\
\left(\frac{\partial}{\partial t}+\Gamma_{10}-i(\omega-\omega_{1E0})\right)\rho_{1E0} &= iG_{12}\rho_{2E0} + iG_{10}\rho_{00},\\
\left(\frac{\partial}{\partial t}+\Gamma_{20}-i(2\omega-\omega_{2E0})\right)\rho_{2E0} &= iG_{21}\rho_{1E0},
\end{aligned} \tag{6}$$

where $\rho_{nn} = \int \rho_{nEnE}\,dE$ is the integral populations of the intermediate ($n=1$) and final ($n=2$) states. We have omitted the terms,

$$-i\int dE_1 \rho_{1E1E_1} G_{10}, \quad -i\int dE_1 \rho_{2E1E_1} G_{10}, \tag{7}$$

in the right-hand side of the fifth and sixth equations of Eq. (6). These terms are related to the emission transitions from the continuum states ψ_E to the $1s$ state. This approximation is valid because the populations of both excited states do not exceed 25%, even for the highest intensities considered (see Sec. III). One can expect that the approximation (7) has a wider region of applicability. Indeed, physical intuitions imply that these transitions from the continuum ψ_E back into the bound state $1s$ could be ignored because the fast photoelectron has enough time to escape the atom, within the lifetime of the hole. The spectral broadening γ in Eq. (5) of the SASE XFEL pulse is about a few eV [4] and significantly exceeds $\Gamma_{ii}/2$. This means that the decay rates of the coherences are close to each other,

$$\Gamma_{20} \approx \Gamma_{10} \approx \Gamma_{21} \approx \gamma. \tag{8}$$

If we use the resonance condition ($\omega = \omega_{21}$), the last two equations in Eq. (6) become

$$\begin{aligned}
\left(\frac{\partial}{\partial t}+\gamma+i(E-\Omega)\right)\rho_{1E0} &= iG_{12}\rho_{2E0} + iG_{10}\rho_{00},\\
\left(\frac{\partial}{\partial t}+\gamma+i(E-\Omega)\right)\rho_{2E0} &= iG_{21}\rho_{1E0}.
\end{aligned} \tag{9}$$

Here, $\Omega = \omega - I_{1s}$ is the detuning of the photon frequency from the K-shell ionization threshold. We then get the following decoupled equations,

$$\dot{R}_+ = iG_{12}R_+ + iG_{10}\rho_{00}, \quad \dot{R}_- = -iG_{12}R_- + iG_{10}\rho_{00} \tag{10}$$

for the auxiliary functions $R_\pm$ defined as $R_\pm = (\rho_{1E0} \pm \rho_{2E0})\exp(zt)$, where $z = \gamma + i(E-\Omega)$. The solutions of these equations are straightforwardly given by

$$\begin{aligned}
\rho_{1E0} &= i\int_{-\infty}^{t} dt_1 e^{z(t_1-t)} G_{10}(t_1)\rho_{00}(t_1)\cos[\theta(t)-\theta(t_1)],\\
\rho_{2E0} &= -\int_{-\infty}^{t} dt_1 e^{z(t_1-t)} G_{10}(t_1)\rho_{00}(t_1)\sin[\theta(t)-\theta(t_1)],
\end{aligned} \tag{11}$$

with $\theta(t) = \int_{-\infty}^{t} dt_1 G_{12}(t_1)$. Using the relation $\int \exp[z(t_1 - t)]\,dE = 2\pi\delta(t_1 - t)$, we obtain the following expressions for the integral coherences $\rho_{10} = \int \rho_{1E0}\,dE$ and $\rho_{20} = \int \rho_{2E0}\,dE$:

$$\rho_{10} = i\pi G_{10}\rho_{00}, \quad \rho_{20} = 0. \tag{12}$$

The integration of the first four equations in Eq. (6) over the photoelectron energy results in the following final density-matrix equations:

$$\begin{aligned}
\left(\frac{\partial}{\partial t}+\Gamma_{22}\right)\rho_{22} &= 2\,\mathrm{Im}(\rho_{21}G_{12}),\\
\left(\frac{\partial}{\partial t}+\Gamma_{11}\right)\rho_{11} &= \gamma_{\mathrm{ph}}\rho_{00} - 2\,\mathrm{Im}(G_{12}\rho_{21}),\\
\left(\frac{\partial}{\partial t}+\Gamma_{21}\right)\rho_{21} &= -i(\rho_{22}-\rho_{11})G_{21},\\
\frac{\partial}{\partial t}(\rho_{00}+\rho_{11}+\rho_{22}) &+ \Gamma_{11}\rho_{11} + \Gamma_{22}\rho_{22} = 0,
\end{aligned} \tag{13}$$

where the K-shell photoionization rate $\gamma_{\mathrm{ph}} = 2\pi|G_{10}|^2$ is defined in same way as in Eq. (4). Equations (13) are in agreement with the simple picture based on the rate equations because the term $-2\,\mathrm{Im}(G_{12}\rho_{21})$ is nothing else than the probability of the transition $|1E\rangle \to |2E\rangle$. Here, one should note that these equations are not only valid for the studied case $\gamma \gg \Gamma_{ii}/2$ Eq. (8). The same result $\rho_{20} \approx 0$ and, hence, Eq. (13) are valid for short ($\tau\Gamma_{i0} \ll 1$) as well as for long ($\tau\Gamma_{i0} \gg 1$) XFEL pulses.

We would like to stress that, in the BCBB scheme, as the x rays first ionize the atom, the bound-bound transition occurring in the second step, both transitions are resonant, as shown schematically in Fig. 1(b). One should note that there exists a competitive TPA channel (i.e., $1s^2 2s^2 2p^6 3p^0 \to 1s^1 2s^2 2p^6 3p^1 \to 1s^0 2s^2 2p^6 3p^1 \psi_E^1$ with the same final state as the BCBB scheme). However, the probability of this channel is significantly smaller than the studied BCBB channel shown

in Fig. 1(b) because the $1s \rightarrow 3p$ transition (occurring in the first step) is off-resonant.

C. Outline of the numerical simulations

Multireference complete-active-space- (CAS-) type wave functions have been used to describe the ground and all relevant excited states of the neon atom. In our computations, we employed two electrons in the $1s3p$ orbitals set [i.e., CAS(4/2)], for the neon atom and one electron in the $1s3p$ orbital set [i.e., CAS(4/1)], for the neon atom cation. Here, CAS(n/m) stands for a CAS, which includes m electrons in n orbitals. This means that configuration space of the CAS wave function is constructed making full configuration interaction expansion for m electrons in n orbitals. Transition dipole moments between state-averaged CAS-type wave functions have been computed using the biorthogonalization procedure implemented in the GAMESS-US program [40]. The electron correlation effects in energetic calculations have been taken into account by using multireference quasidegenerated perturbation theory, which allowed including correlation contribution from electrons not included in CAS space.

Two x-ray photons resonantly excite the atom from the ground state ^1S ($1s^2 2s^2 2p^6$) to two possible final states ^1D and ^1S ($1s^0 2s^2 2p^6 3p^2$) via the off-resonant intermediate state $^1P(1s^1 2s^2 2p^6 3p^1)$. The transition energies and dipole moments are collected in Table I.

The density-matrix equations (3) and (13) are solved numerically with the initial condition $\rho_{00}(-\infty) = 1$ assuming the condition of strict two-photon resonance,

$$2\omega = \omega_{20}, \quad \omega - \omega_{10} = -(\omega - \omega_{21}) = \Omega > 0. \tag{14}$$

The scheme shown in Fig. 1(a), with the off-resonant intermediate state, is performed with a photon frequency of $\omega = 927.66$ eV, while $\omega = 984.7$ eV is set for the scheme shown in Fig. 1(b), where the intermediate continuum state is on-resonance with x-ray photons. According to Table I, the BBBB scheme has two close-lying final states. The simulations for the BBBB scheme were only performed for the ^1D final state. Because the transition energy and the dipole moment to the ^1S final state are very close, very similar results are expected.

In the BCBB scheme [Fig. 1(b)], x rays ionize the atom in the first step ($1s \rightarrow \psi_E$)[$^1S(1s^2 2s^2 2p^6) \rightarrow {}^2S(1s^1 2s^2 2p^6)$], and the bound-bound transition ($1s \rightarrow 3p$) occurs in the second step. The transition energy of the second step [$^2S(1s^1 2s^2 2p^6) \rightarrow {}^2P(1s^0 2s^2 2p^6 3p^1)$] is 984.7 eV, and the corresponding z component of the transition dipole moment is 0.194 429 D. The cross section of the ($1s \rightarrow \psi_E$) ionization ($\sigma_{\rm ph} = 0.229$ Mb) is obtained using the data from Ref. [41].

According to the calculations of Chen [42], the lifetime broadenings full width at half maximum (FWHM) of the single $1s$ hole and of the double $1s$ hole are different

$$\Gamma_{11} \approx 0.27 \text{ eV}, \quad \Gamma_{22} \approx 0.802 \text{ eV}. \tag{15}$$

The main reason for this difference is that the number of Auger decay channels of the double $1s$-core-hole state is twice than in the single $1s$-core-hole state. The contraction of the atomic orbitals due to less electronic screening of the nucleus when an extra core hole exists is another reason for the increase of Γ_{22}. Our simulations are based on the theoretical widths (15), which correspond to lifetimes $\tau_{11} = 1/\Gamma_{11} \approx 2.4$ fs and $\tau_{22} = 1/\Gamma_{22} \approx 0.82$ fs, respectively. One should mention that the experimental values of Γ_{11} of the single $1s$-hole state of Ne are smaller than the theoretical one and vary in the interval 0.24–0.15 eV [43]. Our calculations are performed for an XFEL bandwidth half width at half maximum $\gamma \approx 2$ eV, in agreement with the broadening of the SASE XFEL pulse of about $\gamma/\omega \approx 10^{-3}$ [4].

TABLE I. The transition energies and the z components of the transition dipole moments of the BBBB scheme. The value in brackets is the experimental energy of the $^1S(1s^2 2s^2 2p^6) \rightarrow {}^1P(1s^1 2s^2 2p^6 3p^1)$ transition [11]. ^1S and ^1D are the two core-hole final states $1s^0 2s^2 2p^6 3p^2$. The experimental ionization potential of the $1s$ level is 870.2 eV.

States	Transition energy (eV)	Dipole moment (D)
$^1S \rightarrow {}^1P$	868.39(867.1)	0.225 679
$^1P \rightarrow {}^1D$	986.93	0.119 477
$^1P \rightarrow {}^1S$	987.09	0.085 635

III. DISCUSSION

We will now focus our attention on the population of excited states because the intensity of x-ray emission is directly proportional to the population of the corresponding decaying state.

A. Results of simulations of BBBB scheme

The results of our simulations for different peak intensities I of the Gaussian pulse are collected in Figs. 2–6 for various pulse durations (FWHM) $\tau = 1$, 5, 10, 30, and 100 fs, respectively. These figures show that the dynamics of the population of the TPA and intermediate states are very different when the intensity increases. The population of the TPA

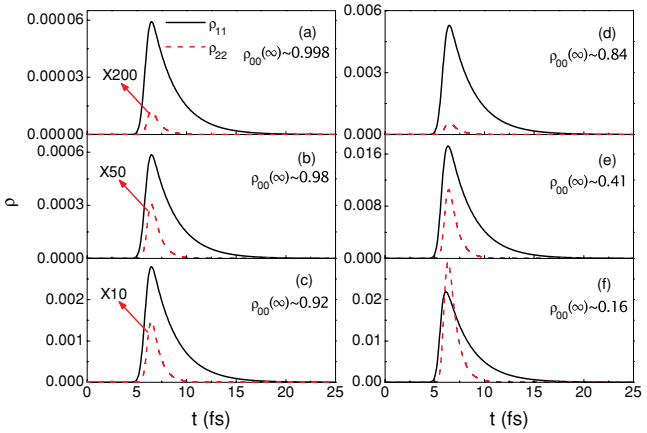

FIG. 2. (Color online) BBBB transition model [Eq. (3)]. Time-dependent population distributions for different XFEL peak intensities: (a) $I = 1 \times 10^{15}$ W/cm^2. (b) $I = 1 \times 10^{16}$ W/cm^2. (c) $I = 5 \times 10^{16}$ W/cm^2. (d) $I = 1 \times 10^{17}$ W/cm^2. (e) $I = 5 \times 10^{17}$ W/cm^2. (f) $I = 1 \times 10^{18}$ W/cm^2. The XFEL frequency is $\omega = 927.66$ eV. The pulse duration (FWHM) is $\tau = 1$ fs.

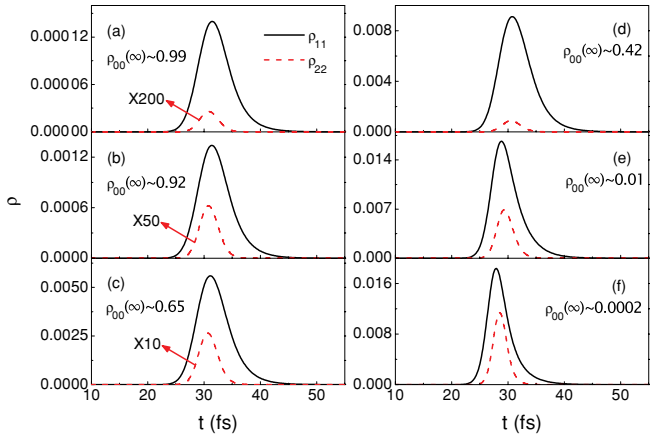

FIG. 3. (Color online) Same as Fig. 2 but for a pulse duration $\tau = 5$ fs.

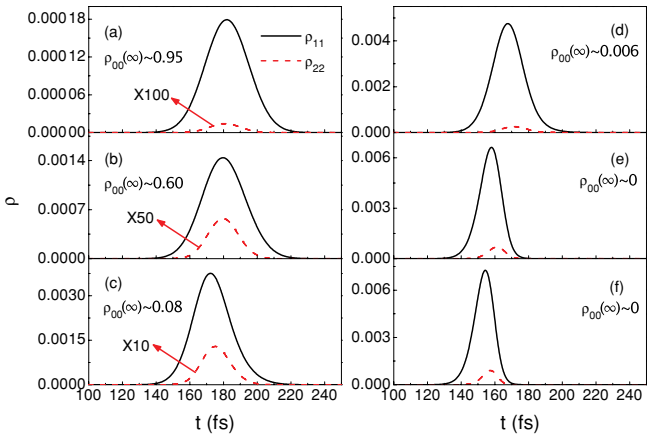

FIG. 5. (Color online) Same as Fig. 2 but for a pulse duration $\tau = 30$ fs.

state is about 0.1% of the intermediate one for low intensity $I = 10^{15}$ W/cm^2. This is mainly due to the rather large spectral width γ of the XFEL pulse. Both the populations of the excited states as well as the ratio ρ_{22}/ρ_{11} increase at higher intensities. One can even see a population inversion for the high intense short pulse [Fig. 2(f), with $\tau = 1$ fs and $I = 10^{18}$ W/cm^2].

More detailed information about the maximum of population ρ_{22} is collected in Fig. 7(a). The pulse begins to promote more than 0.1% of atoms in the TPA state starting from intensity 10^{17} W/cm^2. The population ρ_{22} grows faster for higher intensities.

One should strongly pay attention to the decrease of the concentration of intact molecules $\rho_{00}(\infty)$ due to both direct photoionization and Auger decay [see Eq. (3)]. This depopulation becomes important for peak intensities higher than $I = 5 \times 10^{17}, 5 \times 10^{16}, 5 \times 10^{16}, 1 \times 10^{16}, 1 \times 10^{16}$ W/cm^2 for pulse durations $\tau = 1$, 5, 10, 30, 100 fs, respectively. Here, numerical analysis shows that direct photoionization plays a major role in this effect, which subsequently strongly suppresses the population of the TPA state for long pulses $\tau = 30$ and 100 fs [Fig. 7(a)].

As one can already see from Fig. 1, the transition energies $1s \rightarrow 3p$ are very different in the Ne atom and the Ne^+ ion. Because of such a large shift of the resonant frequencies in ions compared to the neutral ones, one can expect that the TPA will not have a significant impact for ionized Ne atoms.

B. Results of simulations of the BCBB scheme

The state populations for the BCBB scheme differ qualitatively from the BBBB scheme as seen from Figs. 8–12. The main difference resides in the fact that the intermediate continuum state is exactly resonant. Therefore, in contrast to the BBBB scheme (3), the population dynamics is very close to a stepwise process because of the coherence $\rho_{20} \approx 0$, see Eqs. (12) and (13).

One can see that we reach the saturation of the populations on the second (bound-bound) step $\rho_{11} \approx \rho_{22}$ for $I \geqslant 10^{17}$ W/cm^2, except for long pulse (i.e., $\tau = 100$ fs). The main reason for this saturation is the large value of the transition dipole moment of the bound-bound $|1E\rangle \rightarrow |2E\rangle$ transition. Detailed information about the dependence of the maximum value of population ρ_{22} on the pulse duration and peak intensity are again collected in Fig. 7(b). It is important to mention that the BCBB scheme gives a higher population for the TPA state in comparison with the BBBB scheme.

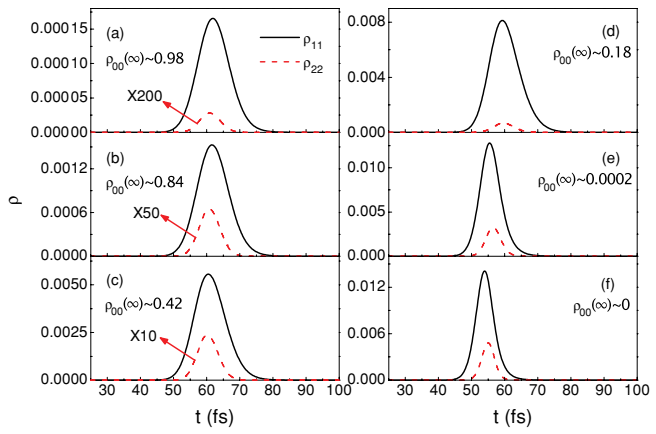

FIG. 4. (Color online) Same as Fig. 2 but for a pulse duration $\tau = 10$ fs.

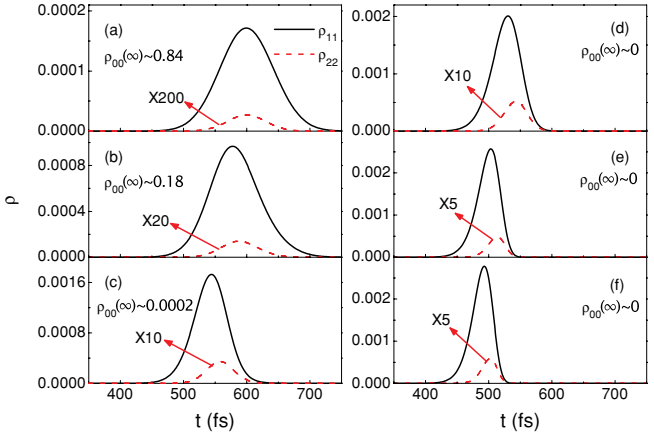

FIG. 6. (Color online) Same as Fig. 2 but for a pulse duration $\tau = 100$ fs.

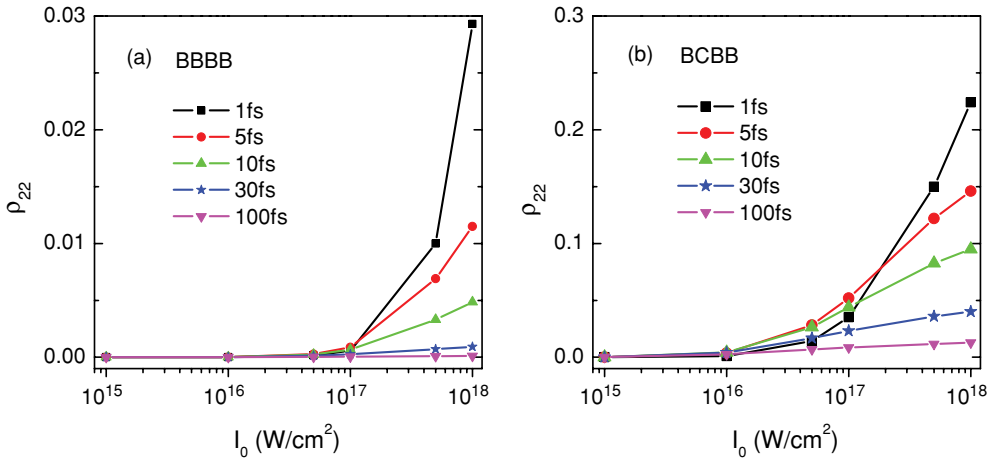

FIG. 7. (Color online) Maximum population of two core-hole states ρ_{22} as a function of XFEL pulse duration and peak intensity. (a) BBBB scheme [Fig. 1(a)]. $\rho_{22} \approx 0.001$ ($\tau = 30$ fs), and $\rho_{22} \approx 0.0001$ ($\tau = 100$ fs) for $I = 1 \times 10^{18}$ W/cm^2. (b) BCBB scheme [Fig. 1(b)].

We will make a special comment on the role of the L-shell ionization. When this ionization is strong enough, TPA can occur in ionized species, and this can result in energy-shifted x-ray emission lines. Figure 13 shows the comparison of the cross sections of ionization of $1s$, $2s$, and $2p$ levels of neon. The calculated cross sections are extracted from Ref. [41]. One can see that the cross section of the K-shell ionization is larger than that of the ionization of the L shell. For example, $\sigma_{2p} : \sigma_{2s} : \sigma_{1s} = 0.023 : 0.046 : 1$ for $\hbar\omega = 927.66$ eV (BBBB scheme) and $\sigma_{2p} : \sigma_{2s} : \sigma_{1s} = 0.022 : 0.044 : 1$ for $\hbar\omega = 984.7$ eV (BCBB scheme). This means that the concentration of the ions ρ_L with the hole in the L shell should be rather small. One can estimate the relative concentration of these ions as

$$w_L = \rho_L/\rho_{00}(-\infty) \approx 1 - e^{-p},$$
$$p = \int dt \gamma_{L,\mathrm{ph}}(t) \approx \tau \gamma_{L,\mathrm{ph}}^{\max} \sqrt{\frac{\pi}{\ln 2}}, \tag{16}$$

where $\gamma_{L,\mathrm{ph}}(t) = \sigma_L I(t)/\hbar\omega$. Using $\sigma_{2s} = 0.01$ Mb and $\sigma_{2p} = 0.005$ Mb, we get $w_L = 0.5(0.3)$, $w_L = 0.07(0.04)$, $w_L = 0.007(0.004)$ for $I = 10^{18}, 10^{17}, 10^{16}$ W/cm^2, respectively, for $\tau = 5$ fs. Here, $w_L = 0.5(0.3)$ means the relative concentration of the ions due to the ionization of the $2s(2p)$ shell.

Already, about 14% of atoms are ionized because of the Auger decay for $I = 10^{17}$ W/cm^2 and $\tau = 1$ fs. The reason for this quenching is the Auger decay of core-ionized states [see Eq. (13)]. The depopulation of the ground state starts to be strong for $\tau \gtrsim 5$ fs, and the pulse ionizes more than 50% of atoms for $I \gtrsim 10^{17}$ W/cm^2. However, as already mentioned earlier, it is difficult to expect that the TPA will be significant for these ions due to the energy-level shifts.

In both TPA schemes [Figs. 1(a) and 1(b)], the x rays off-resonantly also populate the single-core-hole state $1s^1 2s^2 2p^6 3p^1$, which results in the fluorescence $3p \rightarrow 1s$ from this level. This fluorescence ($\hbar\omega_1 = 868.39$ eV) can be distinguished from the fluorescence from the two core-hole final states because the corresponding frequencies are about 120 eV higher [see Figs. 1(a) and 1(b)].

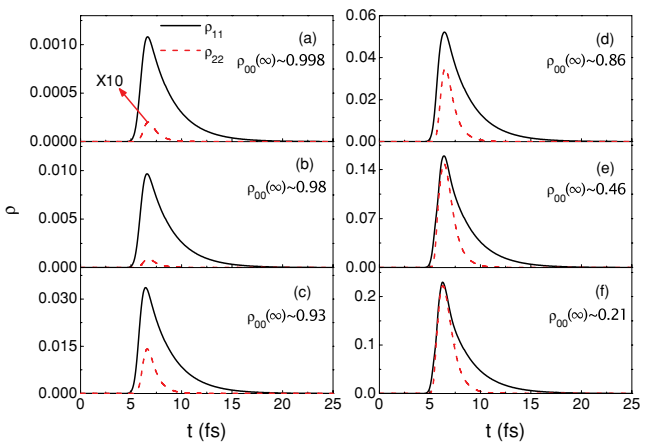

FIG. 8. (Color online) BCBB transition model [Eq. (13)]. Time-dependent population distributions for different XFEL peak intensities: (a) $I = 1 \times 10^{15}$ W/cm^2. (b) $I = 1 \times 10^{16}$ W/cm^2. (c) $I = 5 \times 10^{16}$ W/cm^2. (d) $I = 1 \times 10^{17}$ W/cm^2. (e) $I = 5 \times 10^{17}$ W/cm^2. (f) $I = 1 \times 10^{18}$ W/cm^2. The XFEL frequency is $\omega = 984.7$ eV. The pulse duration (FWHM) is $\tau = 1$ fs.

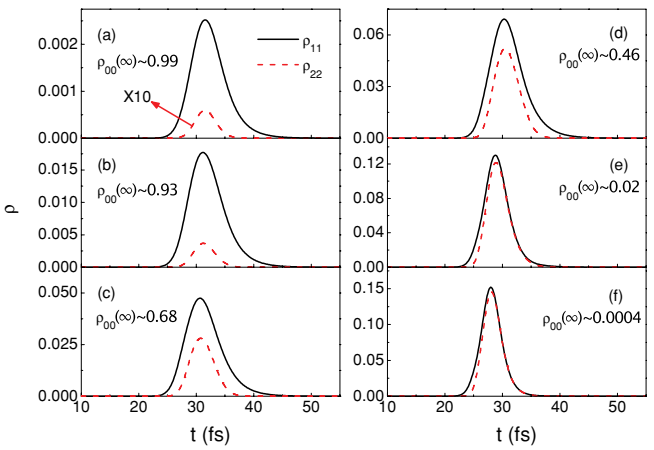

FIG. 9. (Color online) Same as Fig. 8 but for a pulse duration $\tau = 5$ fs.

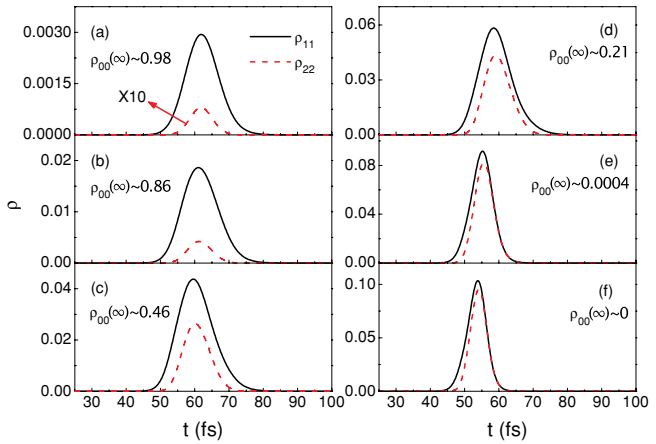

FIG. 10. (Color online) Same as Fig. 8 but for a pulse duration $\tau = 10$ fs.

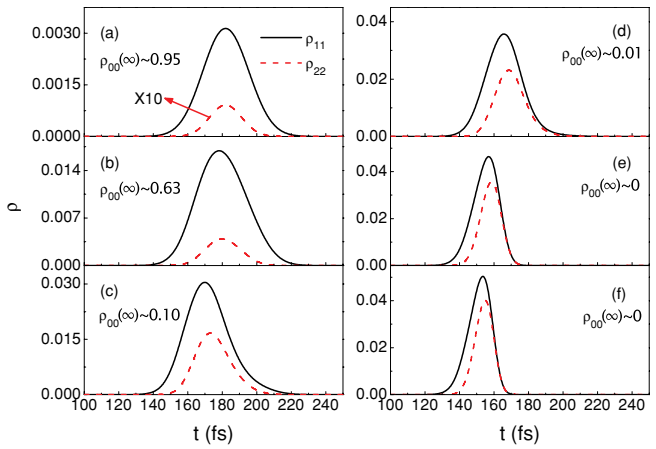

FIG. 11. (Color online) Same as Fig. 8 but for a pulse duration $\tau = 30$ fs.

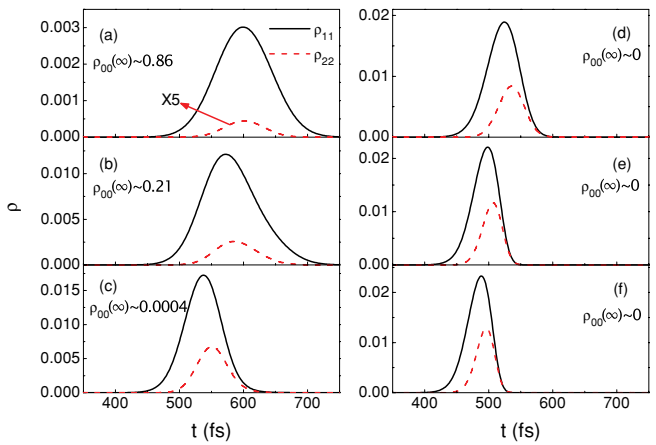

FIG. 12. (Color online) Same as Fig. 8 but for a pulse duration $\tau = 100$ fs.

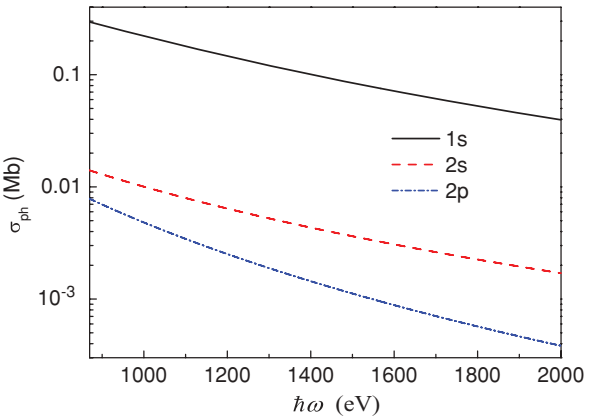

FIG. 13. (Color online) The ionization cross sections of the $1s$, $2s$, and $2p$ electrons of Ne [41].

IV. SUMMARY

High peak intensity of the XFEL allows significant population of the two core-hole states using the two-photon x-ray absorption. Here, we studied two possible schemes of the TPA population of double-hole states in the neon vapors. Both K electrons are excited in the $3p$ orbital because of the TPA of x rays with the frequency 927.66 eV in the first scheme. In the second scheme, the atom is K ionized in the first step and the second $1s$ electron is promoted to the $3p$ atomic orbital by the second x-ray photon. In this case, the photon frequency is higher (984.7 eV). We investigated the dynamics of the population of the final states for different peak intensities and different pulse durations of the XFEL pulse. Significant population of the two core-hole final states results in a rather strong x-ray emission induced by the two-photon x-ray absorption.

According to the LCLS website [44], when the LCLS is operated in short bunch length (low charge) mode, the electron-pulse length is below the 10-fs rms resolution of presently available diagnostics. Based on simulations and indirect measurements, the actual bunch length is expected to be at the level of 1–3-fs rms. The minimum FWHM bandwidth is expected to be 4.5 eV at 900 eV. Intensity as high as 5×10^{17} W/cm^2 is achieved at LCLS for photon energies of 900 eV. Taking the density of the atoms in a supersonic jet into account, the solid angle of the pn-CCD detector and the fluorescence yield, we conclude that x-ray emission of the TPA would give a signal of more than 10^6 count/s.

ACKNOWLEDGMENTS

This work was supported by the Swedish Research Council (VR) and was possible through generous allocations of computer time at the Swedish National Supercomputer Center (NSC) and Center for Parallel Computing (PDC), Sweden. We also acknowledge the Carl Tryggers Foundation, the National Natural Science Foundation of China under Grant No. 10974121, and the National Basic Research Program for China under Grant No. 2006CB806000. Parts of the computations were performed at the Institut du Développement et des Ressources en Informatique Scientifique (IDRIS).

[1] B. Y. Zel'dovich, N. F. Pilipetsky, and V. V. Shkunov, *Principles of Phase Conjugation*, Springer Series in Optical Sciences Vol. 42 (Springer-Verlag, Berlin, 1985).
[2] C. Bressler and M. Chergui, Chem. Rev. **104**, 1781 (2004).
[3] T. Tschentcher, Chem. Phys. **299**, 271 (2004).
[4] [http://xfel.desy.de/science/sti_meeting_2004/].
[5] E. L. Saldin, E. A. Schneidmiller, and M. V. Yurkov, Phys. Rev. ST Accel. Beams **9**, 050702 (2006).
[6] F. F. Guimarães, V. Kimberg, V. C. Felicíssimo, F. Gel'mukhanov, A. Cesar, and H. Ågren, Phys. Rev. A **72**, 012714 (2005).
[7] M. Meyer *et al.*, Phys. Rev. A **74**, 011401 (2006).
[8] J. Schulz *et al.*, Phys. Rev. A **74**, 012705 (2006).
[9] S. Carniato, R. Taïeb, R. Guillemin, L. Journel, M. Simon, and F. Gel'mukhanov, Chem. Phys. Lett. **439**, 402 (2007).
[10] J.-C. Liu, Y. Velkov, Z. Rinkevicius, H. Ågren, and F. Gel'mukhanov, Phys. Rev. A **77**, 043405 (2008).
[11] T. E. Glover *et al.*, Nat. Phys. **6**, 69 (2010).
[12] M. Richter, M. Y. Amusia, S. V. Bobashev, T. Feigl, P. N. Juranic, M. Martins, A. A. Sorokin, and K. Tiedtke, Phys. Rev. Lett. **102**, 163002 (2009) and references therein.
[13] Y.-P. Sun, J.-C. Liu, and F. Gelmukhanov, J. Phys. B **42**, 201001 (2009).
[14] Y.-P. Sun, J.-C. Liu, and F. Gelmukhanov, EPL **87**, 64002 (2009).
[15] Y.-P. Sun, J.-C. Liu, C.-K. Wang, and F. Gelmukhanov, Phys. Rev. A **81**, 013812 (2010).
[16] U. Harbola and S. Mukamel, Phys. Rev. B **79**, 085108 (2009).
[17] J. Arthur *et al.*, LCLS Conceptual Design Report, SLAC-R-593, UC-414, April 2002 [http://ssrl.slac.stanford.edu/lcls/cdr/].
[18] T. Shintake *et al.*, Nat. Photonics **2**, 555 (2008).
[19] European XFEL Technical Design Report No. DESY 2006-097, Hamburg, Germany, 2006, edited by M. Altarelli *et al.*, ISBN: 978-3-935702-17-1.
[20] M. Porro *et al.*, *NSS Conference Record* (IEEE, Piscataway, NJ, 2008), pp. 1578–1586.
[21] H. Ågren, J. Nordgren, L. Selander, C. Nordling, and K. Siegbahn, J. Electron Spectrosc. Relat. Phenom. **14**, 27 (1978).
[22] J. C. Bhalla, J. Phys. B **8**, 2787 (1975).
[23] S. A. Novikov and A. N. Hopersky, J. Phys. B **33**, 2287 (2000).
[24] S. A. Novikov and A. N. Hopersky, J. Phys. B **35**, L339 (2002).
[25] S. A. Novikov and A. N. Hopersky, Radiat. Phys. Chem. **63**, 115 (2002).
[26] R. Santra, N. V. Kryzhevoi, and L. S. Cederbaum, Phys. Rev. Lett. **103**, 013002 (2009).
[27] Y. Nabekawa, H. Hasegawa, E. J. Takahashi, and K. Midorikawa, Phys. Rev. Lett. **94**, 043001 (2005).
[28] L. Young *et al.*, Nature (London) **466**, 56 (2010).
[29] J. Cryan *et al.*, Phys. Rev. Lett. **105**, 083004 (2010).
[30] L. Fang *et al.*, Phys. Rev. Lett. **105**, 083005 (2010).
[31] M. Nagasono *et al.*, Phys. Rev. A **75**, 051406 (2007).
[32] I. I. Sobelman, *Introduction to the Theory of Atomic Spectra* (Pergamon, Oxford/New York, 1972).
[33] N. Allard and J. Kielkopf, Rev. Mod. Phys. **54**, 1103 (1982).
[34] F. Gel'mukhanov, A. Baev, Y. Luo, and H. Ågren, Chem. Phys. Lett. **346**, 437 (2001).
[35] N. Rohringer and R. Santra, Phys. Rev. A **76**, 033416 (2007).
[36] A. Maitland and M. H. Dunn, *Laser Physics* (North-Holland, Amsterdam/London, 1969).
[37] P. Zoller, J. Phys. B **11**, 2825 (1978).
[38] S. Stenholm, *Foundations of Laser Spectroscopy* (Wiley, New York, 1984).
[39] E. L. Saldin, E. A. Schneidmiller, Yu.V. Shvyd'ko, and M. V. Yurkov, Nucl. Instrum. Methods A **475**, 357 (2001).
[40] M. W. Schmidt *et al.*, J. Comput. Chem. **14**, 1347 (1993).
[41] D. A. Verner and D. G. Yakovlev, Astron. Astrophys. Suppl. Ser. **109**, 125 (1995).
[42] M. H. Chen, Phys. Rev. A **44**, 239 (1991).
[43] J. L. Campbell and T. Rapp, At. Data Nucl. Data Tables **77**, 1 (2001).
[44] [https://slacportal.slac.stanford.edu/sites/lclscore_public/Lists/LCLS_FAQ/FAQ.aspx].